JACS Au
AN OPEN ACCESS JOURNAL OF THE AMERICAN CHEMICAL SOCIETY

pubs.acs.org/jacsau

Article

Assembling Silver Cluster-Based Organic Frameworks for Higher-Performance Hypergolic Properties

Chao Wang, Ya-Jie Wang, Chun-Lin He, Qian-You Wang,* and Shuang-Quan Zang

Cite This: *JACS Au* 2021, 1, 2202–2207

Read Online

ACCESS | Metrics & More | Article Recommendations | Supporting Information

ABSTRACT: Increasing research efforts have been focused on developing next-generation propellants. In this work, we demonstrated that assembling zero-dimensional (0D) silver clusters with energetic ligands into 3D metal organic frameworks (MOFs) not only inherited the short ignition delay (ID) time of the alkynyl-silver cluster but also significantly increased the output energy. Among them, the open cationic framework of ZZU-363 incorporating counter NO_3^- ions achieved a considerably reduced energy barrier and eventually the shortest ID time (26 ms), together with the highest volumetric energy density (40.4 kJ cm^{-3}) and specific impulse (263.1 s), which is far superior to traditional hydrazine-based propellants. The underlying mechanisms are clearly revealed by theoretical calculations. This work opens a venue to significantly enhancing the hypergolic activity of metal clusters and MOFs.

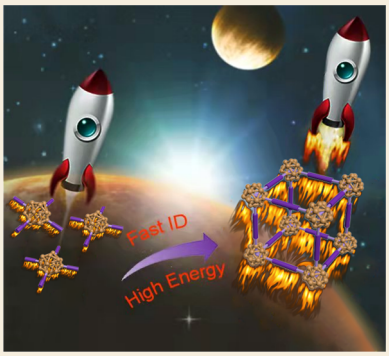

KEYWORDS: *silver cluster, hypergolic fuels, metal−organic frameworks, assembled material, energetic material*

Hypergolic fuel is capable of spontaneous ignition upon contact with an external oxidizer, which serves as the driving force of rocket motors and determines the altitude and range of spacecraft.[1−3] However, currently used hypergolic fuels, such as monomethyl hydrazine (MMH) and unsymmetrical dimethylhydrazine (UDMH), suffer from high toxicity and instability issues.[4−7] Pioneering researchers have devoted significant effort to develop next-generation hypergolic fuel, and the most reported are hypergolic ionic liquids (ILs).[2,8−12] Although ILs feature the advantages of low toxicity and high thermal stability, the intrinsic strong corrosivity of ILs result in great potential safety risks.[13,14] Therefore, the development of a novel hypergolic fuel is a very significant theme but remains challenging.

Recently, we explored the hypergolic behavior of atomically precise metal clusters, in which the inner metal core serves as a hot spot for ignition.[15] In particular, we discovered that the alkynyl-silver bond aids in activating the energetic ligand by lowering the bandgap.[15] Despite the hypergolicity potential of metal clusters,[16−24] 0D metal clusters have only weak van der Waals (vdW) forces acting between the isolated clusters, resulting in low energy storage and specific impulses (*Isp*). Additionally, an in-depth understanding of how hypergolicity is influenced and altered by the structure (including cluster core size, ligands, topology, etc.) is far from clear but holds the key to significantly promoting practical implementation.

As a new class of crystalline hybrid materials featuring well-defined structures and highly tunable components, MOFs hold great promise as molecular platforms to design and synthesize advanced hypergolic propellant candidates.[25−28] In 2019, Rogers and co-workers pioneered the development of a series of hypergolic metal organic frameworks (MOFs) with ultrashort ID times by employing acetylene- and vinyl-substituted imidazole as energetic ligands.[29] However, traditional MOFs with low coordinated ligands per metal hot spot exhibit unsatisfied energy densities, leading to fewer energy loading during the propulsion process. Aiming to combine the advantages of metal clusters and MOFs, we proposed that assembling silver clusters with energetic ligands could produce 3D infinite frameworks (Scheme 1). In contrast to 0D metal clusters, 3D metal cluster-based frameworks with robust coordination bonds and extensive coordinated ligands can significantly increase the output energy and the heats of formation (ΔH_f).[30] More importantly, the extended frameworks facilitates energy transfer,[31,32] and to some extent, the hotspot from the metal clusters early in the ignition process leads to subsequent transfer through the interconnected network, resulting in a fast combustion process with reduced ID time.

In this work, three novel atomically precise silver cluster-based MOFs, $Ag_{12}(PIm)_6(CF_3COO)_6(DMF)_2$ (denoted as ZZU-361), $[Ag_{14}(PIm)_8(CF_3COO)_6]\cdot(DMF)(MeOH)$ (denoted as ZZU-362) and $Ag_{16}(PIm)_8(NO_3)_8$ (denoted as

Received: July 30, 2021
Published: October 11, 2021

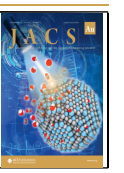

https://doi.org/10.1021/jacsau.1c00334
JACS Au 2021, 1, 2202−2207

Scheme 1. Conceptual Illustrations of 3D Metal Cluster Assembled Materials as Hypergolic Fuels Compared to That of a 0D Metal Cluster

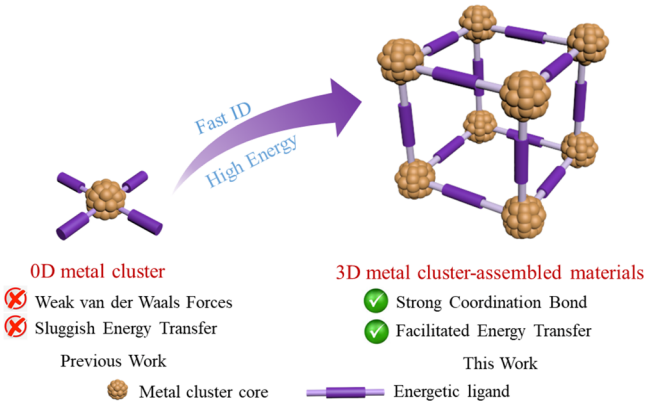

ZZU-363), were obtained by using the energetic ligand 1-propargylimidazole (PIm) as a building block. As expected, the assembly of silver clusters with alkyne moieties or the N atoms of PIm resulted in substantial improvements in hypergolic behavior, including large volumetric energy density, high I_{sp}, short ID time and high ΔH_f. Specifically, a short ID time (26 ms) and high I_{sp} (263.1 s) were achieved for ZZU-363, which was attributed to its interconnecting 1D silver chain and abundant NO_3^- moieties in the framework. Finally, theoretical calculations provided some insights into the structural requirements of high-performance hypergolic materials based on metal cluster assembled materials. The metal cluster core serves as an active site for activating HNO_3 and efficiently reduces the energy barrier. Additionally, ZZU-363 with abundant NO_3^- groups are more beneficial than ZZU-361 or ZZU-362 containing CF_3COO^- groups for excellent ignition performance due to their better bonding ability to HNO_3 and higher nitrogen contents.

Single crystals of the silver cluster-based MOFs were formed via the slow evaporation method from PIm and a silver precursor at room temperature. The detailed synthesis procedures are described in the Supporting Information. Single-crystal X-ray crystallography diffraction (SCXRD) showed that ZZU-361, ZZU-362, and ZZU-363 belong to the $P\bar{1}$, $P2_1/c$, and $P4/ncc$ space groups, respectively, with overall chemical formulas of $Ag_{12}(PIm)_6(CF_3COO)_6(DMF)_2$, $[Ag_{14}(PIm)_8(CF_3COO)_6]\cdot(DMF)(MeOH)$ and $Ag_{16}(PIm)_8(NO_3)_8$, respectively (Figure 1). The asymmetric units of ZZU-361 and ZZU-362 contained half of the formula. In ZZU-361, the Ag_{12} core, which can be described as a hollow cuboctahedron frame and a distributed Ag_3−Ag_6−Ag_3 three-layer arrangement, is similar to that in a previous report.[33] The silver cage is shielded by six PIm ligands and six CF_3COO^- auxiliary ligands. For the Ag_{14} core of ZZU-362, the structure can be described as one Ag_8 octahedron and two Ag_3 triangles, with Ag_8 attached to each side of the Ag_3 unit. The inside of the core was connected by argentophilic interactions with a $Ag^I\cdots Ag^I$ distance of 2.866(6)-3.219(7) Å.[34] The structure of ZZU-363 consists of infinite 1D Ag chains linked together by two connected PIm ligands, resulting in a 3D framework. The asymmetric unit is composed of two Ag ions, one ligand, and one NO_3^- group. Notably, a large number of NO_3^- groups are located on the wall of the 1D silver chains, forming the unique structure that facilitated the ignition reaction (Figures S3−S5).

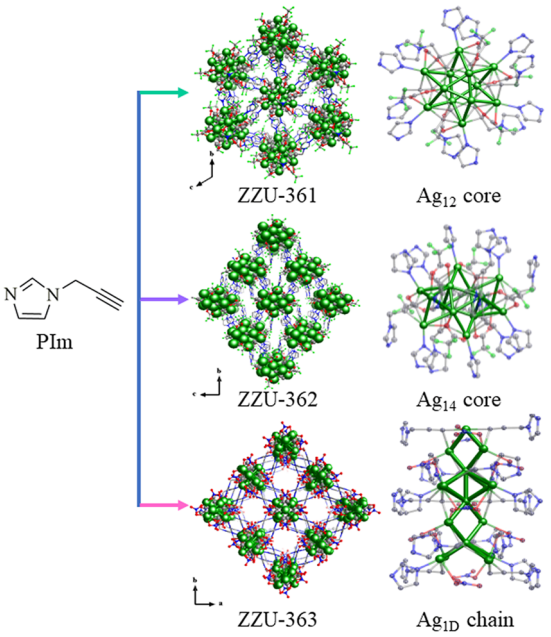

Figure 1. Structures of ZZU-361, ZZU-362, and ZZU-363. The Ag_{12} cluster core in ZZU-361, the Ag_{14} cluster core in ZZU-362, and the Ag_{1D} chain in ZZU-363 are shown on the right. All hydrogen atoms are omitted for clarity, and Ag, C, N, F, and O atoms are shown in green, gray, blue, cyan, and red, respectively.

The phase purity of the three samples was confirmed by comparing the experimental powder X-ray diffraction (PXRD) results to those calculated from the single-crystal structures (Figures S6−8). In addition, Fourier transform infrared attenuated total reflection (FTIR-ATR) spectra were also used to characterize the structural features, and the presence of alkynyl, CF_3COO^-, or NO_3^- moieties in these samples was also observed (Figures S9−11). The water sensitiviies of ZZU-361, ZZU-362, and ZZU-363 were investigated by exposing these samples in different humid environments (relative humidity (RH) = 33, 43, 65, 85, and 98%). The PXRD patterns were well maintained in 3 days, suggesting that the storage life in humid environment ZZU-361, ZZU-362, and ZZU-363 were greater or equal to 3 days (Figures S16−S18). Such good structural stability of these materials lays a foundation for further practical application under different RH conditions. The thermal properties of the materials were measured by thermogravimetric analysis (TGA) with a heating rate of 10 °C min^{-1}. The results indicated all samples displayed good thermostability under both inert and oxidizing conditions (Figures S12−14). Note that ZZU-361 and ZZU-362 showed different mass loss steps under N_2 and O_2 atmospheres. When performed under a N_2 atmosphere, only one major collapse stage was observed at around 150−200 °C, which was assigned to the loss of auxiliary CF_3COO^- ligands and solvent molecules. As for the O_2 atmosphere, the thermal degradation process involved two stages. The first stage was similar to that under a N_2 atmosphere. The second stage at about 420 to 560 °C can be regarded as being due to the oxidization of bridging ligands (PIm) and silver atoms, where the remaining residue mass corresponds to Ag_2O. For ZZU-363, the TGA curves were almost similar under both N_2 and O_2 atmospheres with a drastic energy release at 162.5 °C. According to the TGA curves under a N_2 atmosphere, the onset decomposition temperature for ZZU-361, ZZU-362, and ZZU-363 were

https://doi.org/10.1021/jacsau.1c00334
JACS Au 2021, 1, 2202−2207

Table 1. Calculated Density (ρ_c), Combustion Enthalpy (ΔH_c), Heat of Formation (ΔH_f), Specific Energy (E_g), Energy Density (E_v), and Hypergolic Properties of the Explored Materials Compared to Those of Selected Fuels and Energetic Materials

fuel	ρ^a	$-\Delta H_c{}^b$ (kJ mol^{-1})	E_g (kJ g^{-1})	E_v (kJ cm^{-3})	$\Delta H_f{}^c$ (kJ mol^{-1})	$I_{sp}{}^d$	ID/(ms)	flame duration (ms)	flame height^e (cm)
ZZU-361	2.556	33799.2	12.3	31.4	3025.2	161.4	60	152	7
ZZU-362	2.269	47694.5	15.2	34.5	11835.6	219.6	59	113	7
ZZU-363	2.640	46893.9	15.3	40.4	22051.1	263.1	26	80	>7
CBA-Ag[15]	1.424	72663.0					140		
Zn(VIM)$_2$[25]	0.976	4789.9	19.0	18.9			29	sparks	sparks
Zn(AIM)$_2$[25]	0.996	4783.8	19.3	19.3			2	>600	4
BmimDCA[39]	1.061	6069.0			244.0	244.2	44		
UDMH[37,38]	0.790	1980.1			48.3	239.0[41]	4.8[38]		

[a]Densities obtained from X-ray measurements (g cm^{-3}). [b]Calculated combustion enthalpy (ΔH_c) from their corresponding molecular weights. [c]Heat of formation. [d]Specific impulse (EXPLO5 v6.05.04). [e]Approximate values.

144.4, 190.9, and 162.5 °C, respectively. The differential scanning calorimetry (DSC) curves of the three materials all exhibited an endothermic peak at ∼170 °C (Figure S15), which is consistent with the TGA results. In addition, sensitivity measurements showed that the three MOFs were insensitive to impact and friction (IS > 40 J and FS > 360 N).

Density, combustion energies, and ID times are crucial indicators that define the performance of propellant fuels.[35,36] Higher densities mean that more fuel can be packed into a rocket fuel tank, therefore loading more energy during the propulsion process. The densities of ZZU-361, ZZU-362, and ZZU-363 were 2.556, 2.269, and 2.640 g cm^{-3}, respectively, which are considerably higher than those of known hydrazine fuels (UMMH, 0.79 g cm^{-3}),[37,38] typical hypergolic ILs (BmimDCA, 1.061 g cm^{-3},)[39] and other metal-containing hypergolic fuel (Zn(AIM)$_2$, 0.996 g cm^{-3}).[25] The heats of combustion (ΔH_c) of the three materials were measured by oxygen bomb calorimetry and determined to be −33799.2, −47694.5, and −46893.9 kJ mol^{-1} (Table 1). Then, gravimetric (E_g) and volumetric (E_V) energy densities were computed from ΔH_c. In particular, the E_V values of ZZU-361 (31.4 kJ cm^{-3}), ZZU-362 (34.5 kJ cm^{-3}), and ZZU-363 (40.4 kJ cm^{-3}) were much higher than those of previously reported hypergolic MOFs, Zn(AIM)$_2$ (19.3 kJ cm^{-3}) and Co(AIM)$_2$ (19.5 kJ cm^{-3}).[25]

The hypergolic performance of ZZU-361, ZZU-362, and ZZU-363 with white fuming nitric acid (WFNA) was evaluated by using standard oxidizer-to-fuel droplet tests. In a typical procedure, a single droplet of WFNA (30 μL) was added to a 5 mL tube containing a 15 mg sample. A high-speed camera operating at 1000 frames s^{-1} was used to record the ID time, which is the time between ignition and the first contact of the fuel with the oxidizer. The drop test results are summarized in Table 1. The observed ID times of ZZU-361 and ZZU-362 were 60 and 59 ms, respectively, and the self-sustained ignition duration time lasted more than 100 ms (Figure 2). The similar ID times and combustion behavior of ZZU-361 and ZZU-362 suggested that the metal cluster core size does not significantly affect the hypergolic performance. For ZZU-363, a very short ID time of 26 ms was achieved with WFNA, which satisfies the demands of the desired propellent fuel with an ID time of 50 ms or less.[40] Compared with ZZU-361 and ZZU-362, ZZU-363 underwent more vigorous combustion, with a flame greater than 7 cm in height. This result may be ascribed to the higher nitrogen contents of ZZU-363 than of ZZU-361 and ZZU-362. Overall, ZZU-363, integrating short ID times, a large heat of formation, and a high energy density, is a promising hypergolic candidate for propellent fuel.

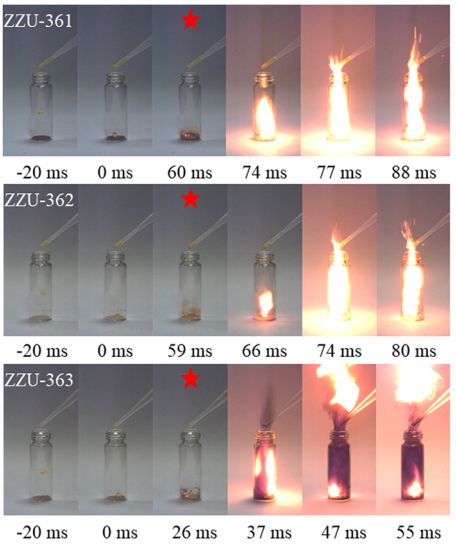

Figure 2. Hypergolicity drop tests with WFNA for ZZU-361 (top), ZZU-362 (middle), and ZZU-363 (bottom).

Notably, the ID times of all these materials are much shorter than that of the previously reported Ag$_{14}$ cluster (CBA-Ag, 140 ms),[15] suggesting that assembling the metal cluster with energetic ligands to produce an infinite frameworks can significantly reduce the ID time. Since the 3D structure can efficiently accelerate the energy transfer process,[31,32] we speculated that the initial hotspot formation around the silver cluster can transfer quickly and trigger the chain reaction in the assembled materials, resulting in a short ID time. In addition, we tried to synthesize a PIm-protected discrete silver cluster as a control sample. However, because both the alkyne group and N atoms of the heterocycle in PIm could coordinate with the silver atom, the desired product was not obtained. To further investigate the critical role of the metal cluster, we performed control experiments involving imidazole (Im), pure ligand (PIm), the metal precursor CF_3COOAg, and $^tBuC{\equiv}CAg$. None of these materials exhibited hypergolic behavior with WFNA, supporting the idea that silver clusters acted as active sites to trigger the hypergolic behavior of silver cluster-based MOFs. Additionally, we conducted droplet tests of the physical mixture of CF_3COOAg, $^tBuC{\equiv}CAg$, and PIm, which showed poor hypergolic performance with an ID time of 200 ms,

https://doi.org/10.1021/jacsau.1c00334
JACS Au 2021, 1, 2202−2207

further confirming that the unique structure of silver cluster-based MOFs contributed to the excellent hypergolic property

Moreover, ΔH_f, which reflects the energetic content of fuel, was calculated by Hess's law and was found to be 3025.2 kJ mol^{-1} for ZZU-361, 11835.6 kJ mol^{-1} for ZZU-362, and 22051.1 kJ mol^{-1} for ZZU-363. Such a high ΔH_f ensured the excellent output energy of these materials. With the calculated ΔH_f, density, and molecular weight, the specific impulse (I_{sp}) was subsequently calculated by means of the EXPLO5 (v6.05.04) program to evaluate the thrust of chemical-based rocket propellants per unit weight. As listed in Table 1, the I_{sp} values of ZZU-361, ZZU-362, and ZZU-363 were 161.4, 219.6, and 263.1 s, respectively. To our delight, the I_{sp} value of ZZU-363 was higher than that of conventional fuels, such as UDMH,[41] and BmimDCA.[39] (Table 1). Because of their different ΔH_f and I_{sp} values, the energetic group contents are considered to be the key influencing factor. The higher PIm ligand ratio in the ZZU-362 structure than in ZZU-361 resulted in larger ΔH_f and I_{sp} values. The ZZU-363 framework contained a large number of NO_3^- moieties in addition to the PIm ligands, leading to a much higher I_{sp} than those of ZUU-361 and ZZU-362.

To more fully understand the difference in the hypergolicity of the three silver cluster-based MOFs and explore the reaction mechanism, we performed density functional theory (DFT) calculations implemented in the Vienna ab initial simulation package (VASP). Considering that the energy gap is associated with the reactivity of the fuel toward the WFNA,[43] we first investigated the bandgap of these materials. As seen in Figures S26–S28, ZZU-361 and ZZU-362 possess wider band gaps of 2.686 and 2.472 eV, respectively. In contrast, ZZU-363 showed a smaller band gap of 1.735 eV (Figure S28). A possible reason for these considerably different bandgaps is the cooperation contribution of their different substituent groups and core structure.[44,45] On the one hand, the stronger electron-withdrawing ability of the CF_3COO^- groups in ZZU-361 and ZZU-362 than of the NO_3^- groups in ZZU-363 results in a larger bandgap. On the other hand, their distinct metal cluster core electronic structures may also be responsible for the different bandgaps.[45] Overall, these observations indicated that ZZU-363 can react more easily with the oxidizer WFNA and presented better hypergolic behavior.

In addition, we studied the electrostatic potential (ESP) on the molecular van der Waals (vdW) surface, which could illustrate the adsorption sites between hypergolic propellants and oxidants and partially explain the ignition performance.[37,42,43] Lower ESP values imply more electronegativity, usually facilitating bonding with the hydrogen of HNO_3 and the corresponding electrophilic reaction.[37] The ESP-mapped vdW surfaces of ZZU-361, ZZU-362, and ZZU-363 are shown in Figure S29. Red represents a low ESP value, whereas blue represents a high ESP value. The results showed that the metal cluster cores of ZZU-361 and ZZU-362 possess higher ESP values than the ligand PIm, which may be ascribed to the strong electron-withdrawing effect of the CF_3COO^- group. This finding implied that ZZU-361 and ZZU-362 have a strong repulsive force against HNO_3, resulting in fewer active sites. When the NO_3^- groups replaced the CF_3COO^- auxiliary ligands in the framework, ZZU-363 displayed a larger area of lower ESP values. Hence, the proton of HNO_3 could easily transfer to the ZZU-363 surface, which is beneficial for the ignition process.

Further, the catalytic mechanism of the hypergolic fuel in the initial ignition process was explored. Three reaction models, $Ag_8(NO_3)_4(PIm)_4$, $Ag_{12}(CF_3COO)_6(PIm)_6(DMF)_2$, and $Ag_{14}(CF_3COO)_6(PIm)_8$, were adopted for the assembled materials (Figure S30). Optimal intermediates and possible reaction pathways for the initial combustion process at room temperature were proposed and are presented in Figure 3. For

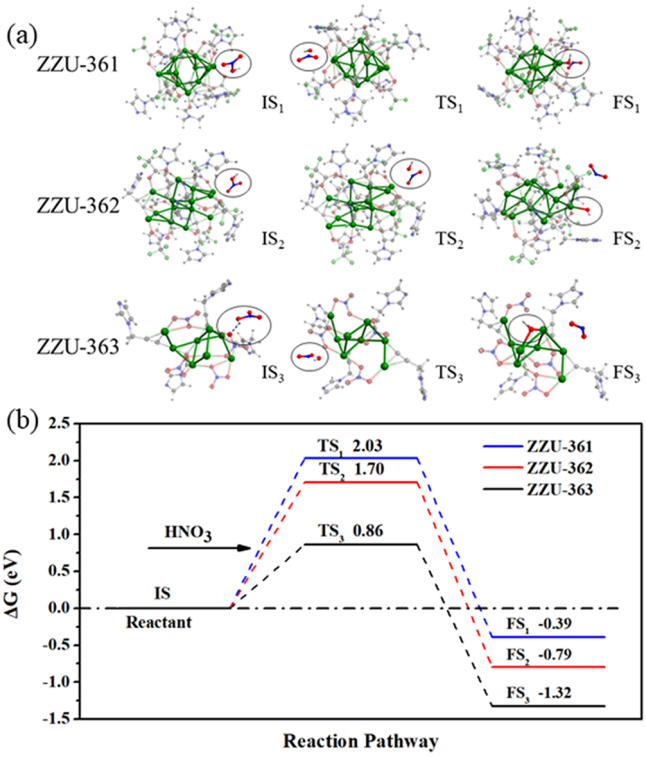

Figure 3. (a) Optimized configurations of intermediates. (b) Calculated free energy diagram of ZZU-361, ZZU-362, and ZZU-363 reacting with HNO_3 molecule at 298 K.

ZZU-361 and ZZU-362, upon introduction of a HNO_3 molecule, the intermediate species TS_1 and TS_2 were formed, and the dissociation of HNO_3 proceeded around the silver cluster during this process. Then, the hydroxy group was bonded with Ag atoms and produced FS_1 and FS_2 intermediates, accompanied by the release of nitrogen oxide (NO_2) gas.[46,47] In contrast to the reaction of ZZU-361 and ZZU-362, for ZZU-363 the hydroxy group of HNO_3 was first bonded with the surface of oxygen atoms of NO_3^- via hydrogen bonds. In this process, ZZU-361 (2.03 eV) and ZZU-362 (1.70 eV) showed a higher energy barrier than ZZU-363 (0.86 eV), implying the lower feasibility of ZZU-361 and ZZU-362 than of ZZU-363. These results indicated that the abundant NO_3^- units in ZZU-363 significantly improved the ignition process. If the initial temperature increases, the process would occur more easily with same reaction path. The free energy diagram of these materials at 2000 K showed lower energy barrier compare to that at 298 K (Figure S31). By combining the experimental results and the above DFT calculations, we conclude that the metal cluster is involved in the reaction with the HNO_3 molecule and initiates the chain reaction.

In conclusion, we have demonstrated that assembling metal clusters with energetic ligands can significantly improve their hypergolic properties. The tunable cluster core size and

https://doi.org/10.1021/jacsau.1c00334
JACS Au 2021, 1, 2202–2207

structure enable fine-tuning of the hypergolic performance. In particular, ZZU-363, which features interconnecting Ag hot spots through Ag−Ag interactions in chains, along with the unique NO_3^- included in the compositions, eventually achieved the shortest ID time (26 ms) and the highest specific impulse (263.1 s). On the basis of the well-defined single-crystal structure, theoretical calculations revealed that the smallest bandgap of ZZU-363 and the strongest affinity of NO_3^- in the oxidizer (HNO_3) are responsible for the superior performance. This work represents an important step toward the development of metal cluster-based hypergolic fuels. The assembled strategy, combined with the various choices of metal clusters and energetic ligands, was expected to allow the development of high-performance metal cluster-based solid propellants for practical application.

■ ASSOCIATED CONTENT

Supporting Information

The Supporting Information is available free of charge at https://pubs.acs.org/doi/10.1021/jacsau.1c00334.

Experimental details and data (PDF)
Data for ZZU-361 (CCDC 2083406) (CIF)
Data for ZZU-362 (CCDC 2083405) (CIF)
Data for ZZU-363 (CCDC 2083407) (CIF)
Video S1 showing the ignition delay process of ZZU-361 (MP4)
Video S2 showing the ignition delay process of ZZU-362 (MP4)
Video S3 showing the ignition delay process of ZZU-363 (MP4)

■ AUTHOR INFORMATION

Corresponding Author

Qian-You Wang − *Henan Key Laboratory of Crystalline Molecular Functional Materials, Henan International Joint Laboratory of Tumor Theranostical Cluster Materials, Green Catalysis Center and College of Chemistry, Zhengzhou University, Zhengzhou 450001, China;* orcid.org/0000-0002-8892-7825; Email: qianyouwang@zzu.edu.cn

Authors

Chao Wang − *Henan Key Laboratory of Crystalline Molecular Functional Materials, Henan International Joint Laboratory of Tumor Theranostical Cluster Materials, Green Catalysis Center and College of Chemistry, Zhengzhou University, Zhengzhou 450001, China*

Ya-Jie Wang − *Henan Key Laboratory of Crystalline Molecular Functional Materials, Henan International Joint Laboratory of Tumor Theranostical Cluster Materials, Green Catalysis Center and College of Chemistry, Zhengzhou University, Zhengzhou 450001, China*

Chun-Lin He − *Chongqing Innovation Center, Beijing Institute of Technology, Chongqing 401120, China;* orcid.org/0000-0002-4099-6477

Shuang-Quan Zang − *Henan Key Laboratory of Crystalline Molecular Functional Materials, Henan International Joint Laboratory of Tumor Theranostical Cluster Materials, Green Catalysis Center and College of Chemistry, Zhengzhou University, Zhengzhou 450001, China;* orcid.org/0000-0002-6728-0559

Complete contact information is available at: https://pubs.acs.org/10.1021/jacsau.1c00334

Notes

The authors declare no competing financial interest.

■ ACKNOWLEDGMENTS

This work was supported by the National Natural Science Foundation of China (92061201, 21825106, and 21901234), the Central Plains Academician Fund of Henan Province (22180017), Henan Science Fund for Excellent Young Scholars (212300410084), the Open Fund of Defense Science and Technology Laboratory (6142602190303), the Program for Innovative Research Team (in Science and Technology) in Universities of Henan Province (19IRTSTHN022), and Zhengzhou University.

■ REFERENCES

(1) Gao, H.; Joo, Y.-H.; Twamley, B.; Zhou, Z.; Shreeve, J. M. Hypergolic Ionic Liquids with the 2,2-Dialkyltriazanium Cation. *Angew. Chem., Int. Ed.* **2009**, *48*, 2792−2795.

(2) Zhang, Y.; Shreeve, J. M. Dicyanoborate-Based Ionic Liquids as Hypergolic Fluids. *Angew. Chem., Int. Ed.* **2011**, *50*, 935−937.

(3) Schneider, S.; Hawkins, T.; Ahmed, Y.; Rosander, M.; Hudgens, L.; Mills, J. Green Bipropellants: Hydrogen-Rich Ionic Liquids that Are Hypergolic with Hydrogen Peroxide. *Angew. Chem., Int. Ed.* **2011**, *50*, 5886−5888.

(4) Pichon, S.; Catoire, L.; Chaumeix, N.; Paillard, C. Search for Green Hypergolic Propellants: Gas-Phase Ethanol/Nitrogen Tetroxide Reactivity. *J. Propul. Power* **2005**, *21*, 1057−1061.

(5) Tani, H.; Terashima, H.; Koshi, M.; Daimon, Y. Hypergolic ignition and flame structures of hydrazine/nitrogen tetroxide co-flowing plane jets. *Proc. Combust. Inst.* **2015**, *35*, 2199−2206.

(6) Bonn, O. D.; Hammerl, A.; Klapötke, T. M.; Mayer, P.; Piotrowski, H.; Zewen, H. Plume Deposits from Bipropellent Rocket Engines: Methylhydrazinium Nitrate and N. *Z. Anorg. Allg. Chem.* **2001**, *627*, 2011−2015.

(7) Wang, K.; Liu, T.; Jin, Y.; Huang, S.; Petrutik, N.; ShemTov, D.; Yan, Q.-L.; Gozin, M.; Zhang, Q. Tandem-action" ferrocenyl iodocuprates promoting low temperature hypergolic ignitions of "green" EIL−H2O2 bipropellants. *J. Mater. Chem. A* **2020**, *8*, 14661−14670.

(8) Smiglak, M.; Metlen, A.; Rogers, R. D. The Second Evolution of Ionic Liquids: From Solvents and Separations to Advanced Materials-Energetic Examples from the Ionic Liquid Cookbook. *Acc. Chem. Res.* **2007**, *40*, 1182−1192.

(9) Zhang, Q.; Shreeve, J. M. Energetic Ionic Liquids as Explosives and Propellant Fuels: A New Journey of Ionic Liquid Chemistry. *Chem. Rev.* **2014**, *114*, 10527−10574.

(10) Li, X.; Wang, C.; Li, H.; Nie, F.; Yin, H.; Chen, F.-X. Bishydrobis(tetrazol-1-yl) borate (BTB) based energetic ionic liquids with high density and energy capacity as hypergolic fuels. *J. Mater. Chem. A* **2017**, *5*, 15525−15528.

(11) Zhang, X.; Pan, L.; Wang, L.; Zou, J.-J. Review on synthesis and properties of high-energy-density liquid fuels: Hydrocarbons, nanofluids and energetic ionic liquids. *Chem. Eng. Sci.* **2018**, *180*, 95−125.

(12) Jiao, N.; Zhang, Y.; Liu, L.; Shreeve, J. M.; Zhang, S. IL-oxidizer/IL-fuel combinations as greener hypergols. *New J. Chem.* **2019**, *43*, 1127−1129.

(13) Wang, Y.-C.; Lee, T. C.; Lin, J. Y.; Chang, J. K.; Tseng, C. M. Corrosion properties of metals in dicyanamide-based ionic liquids. *Corros. Sci.* **2014**, *78*, 81−88.

(14) Uerdingen, M.; Treber, C.; Balser, M.; Schmitt, G.; Werner, C. Corrosion behaviour of ionic liquids. *Green Chem.* **2005**, *7*, 321−325.

(15) Wang, Q.-Y; Wang, J.; Wang, s.; Wang, Z.-Y.; Cao, M.; He, C.-L.; Yang, J.-Q.; Zang, S. Q.; Mak, T. C. W. o-Carborane-Based and Atomically Precise Metal Clusters as Hypergolic Materials. *J. Am. Chem. Soc.* **2020**, *142*, 12010−12014.

(16) Lei, Z.; Wan, X.-K.; Yuan, S.-F.; Guan, Z.-J.; Wang, Q.-M. Alkynyl Approach toward the Protection of Metal Nanoclusters. *Acc. Chem. Res.* **2018**, *51*, 2465−2474.
(17) Konishi, K.; Iwasaki, M.; Shichibu, Y. Phosphine-Ligated Gold Clusters with Core+Exo Geometries: Unique Properties and Interactions at the Ligand−Cluster Interface. *Acc. Chem. Res.* **2018**, *51*, 3125−3133.
(18) Ghosh, A.; Mohammed, O. F.; Bakr, O. M. Atomic-Level Doping of Metal Clusters. *Acc. Chem. Res.* **2018**, *51*, 3094−3103.
(19) Hyeon, T.; Bootharaju, M. S.; Lee, S.; Deng, G.; Malola, S.; Baek, W.; Häkkinen, H.; Zheng, N. Ag44(EBT)26(TPP)4 Nanoclusters with Tailored Molecular and Electronic Structure. *Angew. Chem.* **2021**, *133*, 9120−9126.
(20) Du, Y. X.; Sheng, H. T.; Astruc, D.; Zhu, M. Z. Atomically Precise Noble Metal Nanoclusters as Efficient Catalysts: A Bridge between Structure and Properties. *Chem. Rev.* **2020**, *120*, 526−622.
(21) Yao, Q.; Chen, T.; Yuan, X.; Xie, J. Toward Total Synthesis of Thiolate-Protected Metal Nanoclusters. *Acc. Chem. Res.* **2018**, *51*, 1338−1348.
(22) Zhou, M.; Higaki, T.; Hu, G.; Sfeir, M. Y.; Chen, Y.; Jiang, D.-E.; Jin, R. Three-orders-of-magnitude variation of carrier lifetimes with crystal phase of gold nanoclusters. *Science* **2019**, *364*, 279−282.
(23) Takano, S.; Ito, S.; Tsukuda, T. Efficient and Selective Conversion of Phosphine-Protected (MAu8)2+ (M = Pd, Pt) Superatoms to Thiolate-Protected (MAu12)6+ or Alkynyl Protected (MAu12)4+ Superatoms via Hydride Doping. *J. Am. Chem. Soc.* **2019**, *141*, 15994−16002.
(24) Kalenius, E.; Malola, S.; Matus, M. F.; Kazan, R.; Bürgi, T.; Häkkinen, H. Experimental Confirmation of a Topological Isomer of the Ubiquitous Au25(SR)18 Cluster in the Gas Phase. *J. Am. Chem. Soc.* **2021**, *143*, 1273−1277.
(25) Titi, H. M.; Arhangelskis, M.; Katsenis, A. D.; Mottillo, C.; Ayoub, G.; Do, J. L.; Fidelli, A. M.; Rogers, R. D.; Friščić, T. Metal−Organic Frameworks as Fuels for Advanced Applications: Evaluating and Modifying the Combustion Energy of Popular MOFs. *Chem. Mater.* **2019**, *31*, 4882−4888.
(26) Xu, Y.; Wang, Y.; Zhong, Y.; Lei, G.; Li, Z.; Zhang, J.; Zhang, T. High-Energy Metal−Organic Frameworks with a Dicyanamide Linker for Hypergolic Fuels. *Inorg. Chem.* **2021**, *60*, 5100−5106.
(27) Furukawa, H.; Cordova, K. E.; O'Keeffe, M.; Yaghi, O. M. The Chemistry and Applications of Metal-Organic Frameworks. *Science* **2013**, *341*, 1230444.
(28) Chen, P.; Tang, Z.; Zeng, Z.; Hu, X.; Xiao, L.; Liu, Y.; Qian, X.; Deng, C.; Huang, R.; Zhang, J.; Bi, Y.; Lin, R.; Zhou, Y.; Liao, H.; Zhou, D.; Wang, C.; Lin, W. Machine-Learning-Guided Morphology Engineering of Nanoscale Metal-Organic Frameworks. *Matter* **2020**, *2*, 1651−1666.
(29) Titi, H. M.; Marrett, J. M.; Dayaker, G.; Arhangelskis, M.; Mottillo, C.; Morris, A. J.; Rachiero, G. P.; Friscic, T.; Rogers, R. D. Hypergolic Zeolitic Imidazolate Frameworks (ZIFs) as NextGeneration Solid Fuels: Unlocking the Latent Energetic Behavior of ZIFs. *Sci. Adv.* **2019**, *5*, aav9044.
(30) Qin, J. S.; Zhang, J.-C.; Zhang, M.; Du, D. Y.; Li, J.; Su, Z. M.; Wang, Y. Y.; Pang, S. P.; Li, S. H.; Lan, Y. Q. A Highly Energetic N-Rich Zeolite-Like Metal-Organic Framework with Excellent Air Stability and Insensitivity. *Adv. Sci.* **2015**, *2*, 1500150.
(31) Zhang, Q.; Zhang, C.; Cao, L.; Wang, Z.; An, B.; Lin, Z.; Huang, R.; Zhang, Z.; Wang, C.; Lin, W. Forster Energy Transport in Metal-Organic Frameworks Is Beyond Step-by-Step Hopping. *J. Am. Chem. Soc.* **2016**, *138*, 5308−5315.
(32) Cao, L.; Lin, Z.; Shi, W.; Wang, Z.; Zhang, C.; Hu, X.; Wang, C.; Lin, W. Exciton Migration and Amplified Quenching on Two-Dimensional Metal-Organic Layers. *J. Am. Chem. Soc.* **2017**, *139*, 7020−7029.
(33) Huang, R. W.; Dong, X. Y.; Yan, B. J.; Du, X. S.; Wei, D. H.; Zang, S. Q.; Mak, T. C. W. Tandem Silver Cluster Isomerism and Mixed Linkers to Modulate the Photoluminescence of Cluster-Assembled Materials. *Angew. Chem., Int. Ed.* **2018**, *57*, 8560−8566.
(34) Schmidbaur, H.; Schier, A. Argentophilic Interactions. *Angew. Chem., Int. Ed.* **2015**, *54*, 746−784.
(35) Bhosale, V. K.; Jeong, J.; Choi, J.; Churchill, D. G.; Lee, Y.; Kwon, S. Additive-promoted hypergolic ignition of ionic liquid with hydrogen peroxide. *Combust. Flame* **2020**, *214*, 426−436.
(36) Titi, H. M.; Arhangelskis, M.; Rachiero, G. P.; Friscic, T.; Rogers, R. D. Hypergolic Triggers as Co-crystal Formers: Cocrystallization for Creating New Hypergolic Materials with Tunable Energy Content. *Angew. Chem., Int. Ed.* **2019**, *58*, 18399−18404.
(37) Yuan, W. L.; Zhang, L.; Tao, G. H.; Wang, S. L.; Wang, Y.; Zhu, Q. H.; Zhang, G. H.; Zhang, Z.; Xue, Y.; Qin, S.; He, L.; Shreeve, J. M. Designing high-performance hypergolic propellants based on materials genome. *Sci. Adv.* **2020**, *6*, eabb1899.
(38) Durgapal, U. C.; Venugopal, V. K. Hypergolic Ignition of Rocket Propellants with Nitric Acid Containing Dissolved Nitrogen Tetroxide. *AIAA J.* **1974**, *12*, 1611−1612.
(39) Sun, C.; Tang, S.; Zhang, X. Role of Cation Structures for Energetic Performance of Hypergolic Ionic Liquids. *Energy Fuels* **2017**, *31*, 10055−10059.
(40) Li, S.; Gao, H.; Shreeve, J. M. Borohydride ionic liquids and borane/ionic-liquid solutions as hypergolic fuels with superior low ignition-delay times. *Angew. Chem., Int. Ed.* **2014**, *53*, 2969−2972.
(41) Bhosale, V. K.; Kulkarni, P. S. Propellants, Hypergolic Behavior of Pyridinium Salts Containing Cyanoborohydride and Dicyanamide Anions with Oxidizer RFNA. *Propellants, Explos., Pyrotech.* **2016**, *41*, 1013−1019.
(42) Huang, S.; Qi, X.; Liu, T.; Wang, K.; Zhang, W.; Li, J.; Zhang, Q. Towards Safer Rocket Fuels: Hypergolic Imidazolylidene-Borane Compounds as Replacements for Hydrazine Derivatives. *Chem. - Eur. J.* **2016**, *22*, 10187−10193.
(43) Jin, Y.; Shi, Y.; Qi, X.; Huang, S.; Zhang, Q. Theoretical Study on Hydrolytic Stability of Borohydride-Rich Hypergolic Ionic Liquids. *J. Phys. Chem. A* **2020**, *124*, 2942−2950.
(44) Teunissen, J. L.; De Proft, F.; De Vleeschouwer, F. Tuning the HOMO−LUMO Energy Gap of Small Diamondoids Using Inverse Molecular Design. *J. Chem. Theory Comput.* **2017**, *13*, 1351−1365.
(45) Gutrath, B. S.; Schiefer, F.; Homberger, M.; Englert, U.; Serb, M. D.; Bettray, W.; Beljakov, I.; Meded, V.; Wenzel, W.; Simon, U. Molecular and Electronic Structure of the Cluster [Au8(PPh3)8](NO3)2. *Eur. J. Inorg. Chem.* **2016**, *2016*, 975−981.
(46) Johnston, H. S.; Foering, L.; White, J. R. Kinetics of the Thermal Decomposition of Nitric Acid Vapor. III. Low Pressure Results. *J. Am. Chem. Soc.* **1955**, *77*, 4208−4212.
(47) Laufs, S.; Kleffmann, J. Investigations on HONO formation from photolysis of adsorbed HNO_3 on quartz glass surfaces. *Phys. Chem. Chem. Phys.* **2016**, *18*, 9616−9625.

https://doi.org/10.1021/jacsau.1c00334
JACS Au 2021, 1, 2202−2207